Active Yaw Control of a Ducted Fan-Based MAV using Synthetic Jets

Kiyoshi Otani[1], Joseph Moore[2], William Gressick[2], and Michael Amitay[3]
[1]National Defense Academy, School of Systems Engineering, Department of Aerospace Engineering, Hashirimizu 1-10-20, Yokosuka, Kanagawa, Japan 239-8686
[2]Center for Automation Technologies and Systems, Rensselaer Polytechnic Institute, Troy, NY
[3]Mechanical, Aerospace and Nuclear engineering, Rensselaer Polytechnic Institute, Troy, NY. Corresponding Author; E-mail: amitam@rpi.edu

ABSTRACT

The feasibility of using active flow control to stabilize a micro ducted fan unmanned aerial vehicle in a yaw motion was investigated experimentally. Flow control was implemented using synthetic jet actuators to manipulate the flow around the vehicle's stator vanes. As a result, this mechanically simplified control approach can be used to generate a yaw moment on the vehicle instead of moving control surfaces and articulated rotor blades. The rotational control of the MAV (165.5mm in diameter and 177.8mm in height) was obtained by activating surface-mounted synthetic jets that were mounted on a set of four fixed stators downstream of the duct. The synthetic jets were located downstream of a deliberately formed local separation to enable controlled flow reattachment. The flow field around the stators and in the wake was studied using particle image velocimetry (PIV) where the geometrical angle of attack of the stators was either 0° or 6° and the propeller rotational speed was either 4,200RPM or 9,000RPM (generating a thrust of 2.2N or 8.8N, respectively). The torque generated by the propeller and the counter-torque induced by the combined stators-synthetic jets was measured using a load cell. Activation of the synthetic jets resulted in a partial or a full flow reattachment and thus induced a controlled change to the lift and drag forces on the stators. The modification of the aerodynamic forces yielded a rotational torque that can counteract the torque generated by the propeller. A closed-loop controller with gyroscopic feedback was implemented to regulate the yaw rate to zero and reject disturbances caused by changes in propeller speed.

1. INTRODUCTION

Unmanned Aerial Vehicles (UAVs) are remotely piloted or self-piloted aircraft that can carry cameras, sensors, communications equipment or other payloads. They possess much potential for the ever-growing technological world. They have been used in a reconnaissance and intelligence-gathering role since the 1950s, and more challenging roles are underway, including combat missions, search and rescue, etc. To effectively support the field troops, smaller UAVs have been designed, ranging from backpackable systems to insect-sized "mesicopters", and miniature "smart dust" sensors. They can be launched by hand, deployed by larger UAVs, or ejected from artillery or mortar projectiles, as expendable sensors. These systems are broadly designated as Miniature Aerial Vehicles (MAV). MAVs offer low cost flights, portability, and simplicity of operation. It is therefore an important task to fully understand and develop the control of the MAV. The present work concentrates on a Vertical Take Off and Landing (VTOL) MAV with a ducted fan configuration, where the vehicle control is envisioned to be enabled by actively controlling the flow field, via synthetic jet fluidic actuators.

The control of a ducted fan UAV is typically obtained by using control vanes or counter-rotating rotors. In 1986, Sikorsky Aircraft Corporation started their development on its Cypher UAV (Cycon, 1992 and Walsh & Cycon, 1998.), which uses two coaxial counter-rotating rotors for control and stabilization through collective and cyclic pitch on the blades to control the forces and moments on the vehicle.

Another ducted fan UAV (iSTAR, Adams et al., 2001) was developed by Micro Craft Incorporated and is currently produced by Honeywell. The propulsion of the iSTAR is generated by a two-blade propeller, where eight fixed stators are placed downstream of the propeller to reduce the torque. The directional control of the craft is provided by the control vanes attached to the trailing edge of the stators.

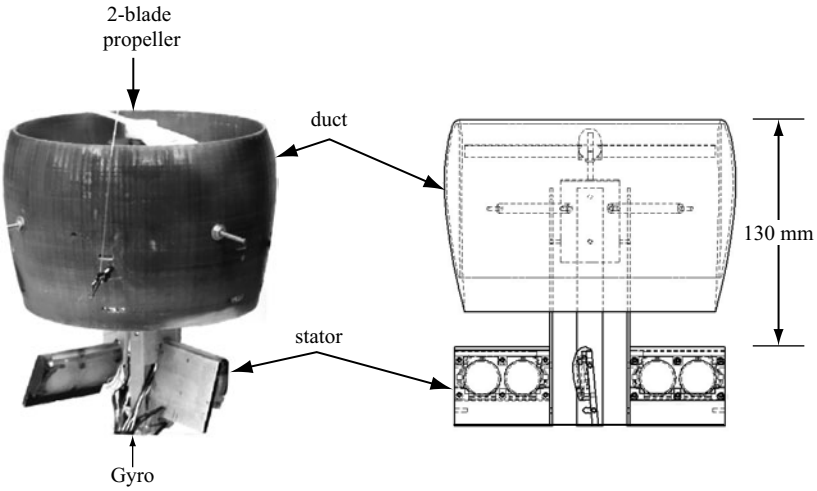

Figure 1. Micro Aerial Vehicle.

Kondor & Heiges (2001) used steady jet injection via a pneumatic blowing ring mounted on the base of the duct to control the flow around the duct. In addition, four fixed stator vanes were installed to partially counter the torque due to the main rotor and provide structural support of the body. More recently, Fung and Amitay (2002) applied active flow control, via synthetic jet actuators, to control the direction and rotation of the vehicle. They studied the flow field around the stator vanes using particle image velocimetry (PIV) at different radial locations, where the geometrical angle of attack of the stator vanes is fixed at 10° and the propeller rotational speed is either 4300 RPM or 6200 RPM. Velocity measurements in the near wake revealed that the flow is quasi-steady.

The use of synthetic (zero mass flux) jet actuators for controlling the flow around airfoils was demonstrated in the past by multiple investigators (e.g., Amitay et al., 2001) where the suppression of separation over an unconventional airfoil at moderate Reynolds numbers (up to 10^6) was obtained, which resulted in a dramatic increase in lift and a corresponding decrease in pressure drag. In their work, Amitay et al. operated the synthetic jets at frequencies that were an order of magnitude higher than the characteristic (shedding) frequency of the airfoil. Therefore, the interaction of the synthetic jets with the cross flow led to local modification of the "apparent" aerodynamic shape of the flow surface, and, as a result, to full or partial reattachment of the separated flow.

Most of the work on flow control has been focused on separation control (i.e., high angles of attack or large flap deflection). However, at low angles of attack, where the flow is fully attached, conventional techniques have little to no effect. Chatlynne et al. (2001) and Amitay et al. (2001) utilized synthetic jet actuators for the concept of virtual aero-shaping. The work was performed on a thick (24%) two-dimensional Clark-Y airfoil model at low angles of attack where the baseline flow is completely attached to the surface of the airfoil. Their idea was to activate a synthetic jet actuator that was placed downstream of a passive obstruction to form a recirculating domain. The formation of this domain altered the streamline resulting in the modification of the apparent shape of the airfoil, and improving the aerodynamic performance of the airfoil at low angles of attack.

In the present paper, the feasibility of flow control (via synthetic jet actuators) to manipulate the flow over the stators of a ducted fan Micro Aerial Vehicle to enable vehicle control is addressed. It is anticipated that controlling the flow over the stators will result in alteration of the aerodynamic forces on the vanes, which in return will alter the forces and moment around the entire vehicle. The expected advantage of this approach is to increase the frequency response of the vehicle, reduce its weight and make it less complex with minimal number of moving parts.

2. EXPERIMENTAL SETUP AND PROCEDURE

The experiments were conducted in the Flow Control Research Lab at RPI. The MAV model that is discussed in the present paper was designed for ground testing, where its weight is not a concern, and thus it was constructed from Stereolithography. The MAV has an overall diameter of 165mm and a total

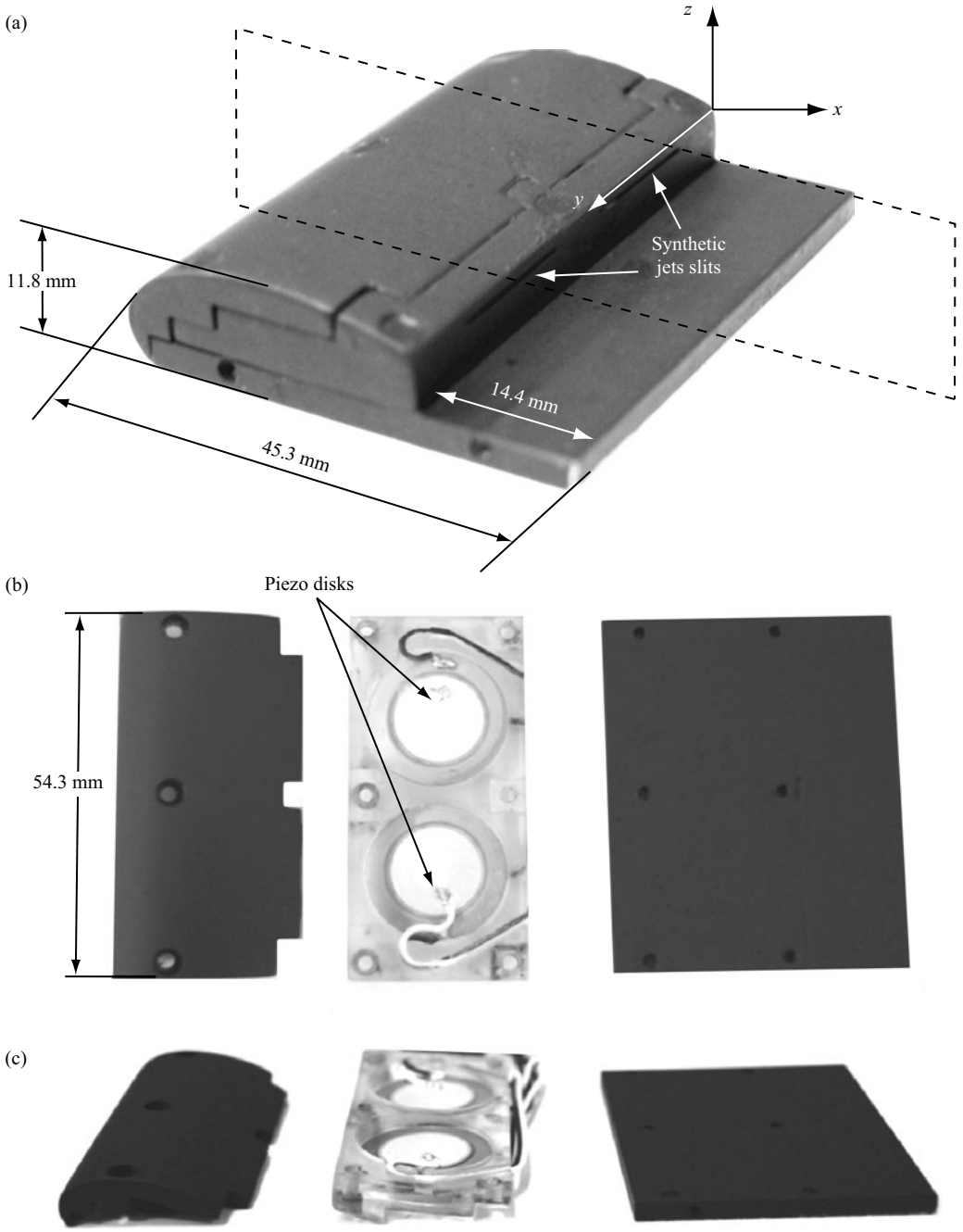

Figure 2. Instrumented stator vane: (a) assembled, (b) top view, and (c) side view.

height of 177.8mm (Figure 1.) The model consists of a propeller and four stator vanes that are placed downstream of the duct. The stators have a modified GOE-435 airfoil shape (having a chord of 45.3mm and a maximum thickness of 11.8mm) where a portion of its upper surface is removed to induce local flow separation (Figure 2). Each stator has a span of 54.3mm and is instrumented with two individually addressable synthetic jet actuators (having a length of 15mm and a width of 0.5mm). Each synthetic jet actuator is driven by a pair of 20mm piezo-ceramic disks that are pre-selected to have the same resonance frequency. For detailed description of the synthetic jet actuator see Smith & Glezer (1998), Glezer & Amitay (2002) and Amitay & Cannelle (2006). The stator vanes are attached to the motor mount, and their leading edge is located 22.5mm downstream of the duct outlet (when the stators are at angle of attack of 0^o). The model is attached to a frame such that it is 1m above the ground to minimize ground effects.

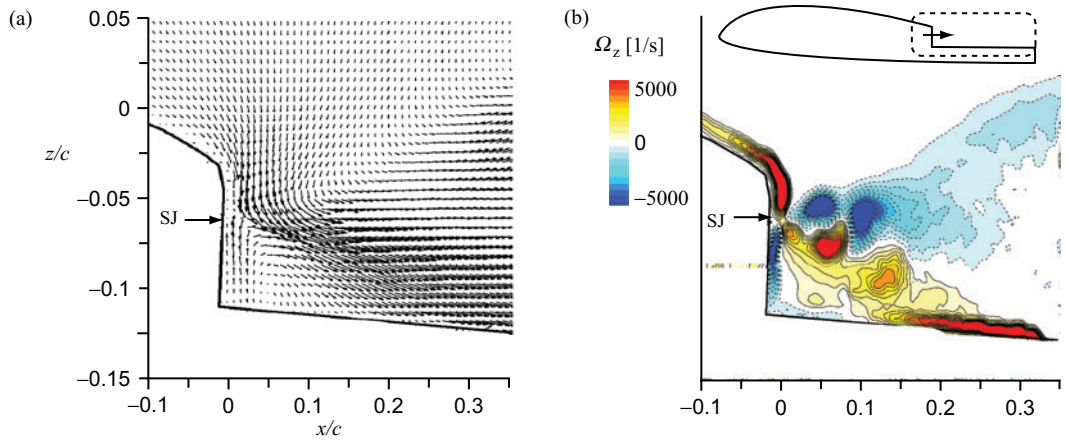

Figure 3. Synthetic jet flow field: (a) time averaged, (b) phase averaged.

The flow within the duct is produced by a commercial off-the-shelf two-blade propeller for model airplanes, and is driven by a brushless DC motor. The motor controller is regulated by a pulse-train waveform, where the rotational speed is varied by changing the width of the pulse.

The flow field around the stators and in their near wake was measured using a Particle Image Velocimetry (PIV) system. A LaVision system, consisting of a high resolution CCD camera, a pair of 120mJ pulsed Nd:YAG lasers, and a programmable timing unit, was used in the current study. Incense smoke (having particles size of a few microns in diameter) was used as tracers, where 250 image pairs were acquired for each case. The PIV velocity vectors were calculated using a cross-correlation technique with adaptive multi-pass, deformable interrogation windows (64×64 to 32×32 pixels), and 50% overlap. The camera was mounted at a perpendicular distance of ~0.4m to the laser light sheet such that the distance between pixels is ~27.1μm. The maximum particle displacement is approximately 7 pixels with an error of approximately ±0.1 pixels, resulting in a velocity uncertainty of ±3% and ±5% uncertainly in the vorticity.

The synthetic jet actuator performance is quantified using the momentum coefficient, c_μ, which is the ratio of the synthetic jet momentum flux to the free-stream momentum flux,

$$c_\mu = \frac{n \cdot \rho_j \cdot l_j \cdot h \cdot U_j^2}{\frac{1}{2} \cdot \rho_0 \cdot \pi \cdot R^2 \cdot U_\infty^2} \tag{1}$$

where ρ_j and ρ_o are the jet and free-stream fluid densities, respectively; h and l_j are the jet orifice width and length, respectively; n is the number of activated jets, R = 141mm is the inner diameter of the duct at its exit plane, U_j is the jet average orifice velocity (based on the blowing portion of the cycle, see Smith & Glezer 1998), and U_∞ is the averaged velocity at the duct exit plane. In the experiments presented here the synthetic jet is actuated at 1,700Hz, and C_μ = 0.065 and 0.012 for ω = 4,200 and 9,000RPM, respectively. The momentum ratio is somewhat high; however, since the synthetic jets operate near resonance their consumed power is ~0.1W per disk, which makes this technique practical.

For the closed-loop control experiments, the experimental system consists of the micro air vehicle, the test fixture, and the electronics and computer to control the vehicle. The electronics hardware is designed specifically for the purpose of controlling synthetic jet actuators, and consists of a microcontroller-based signal generator that is capable of performing amplitude modulation of the sinusoidal waveform. A high-voltage amplifier converts this signal to a level suitable for driving the actuators. The vehicle is equipped with a single-axis MEMS gyroscope from Analog Devices that outputs an analog voltage proportional to the yaw rate in the body frame. A speed controller controls the current to the vehicle motor. The control computer is a conventional PC with analog input and output capability using I/O cards from Measurement Computing. xPC Target, a real-time operating system by the Mathworks, was installed on the PC to enable a rapid prototyping

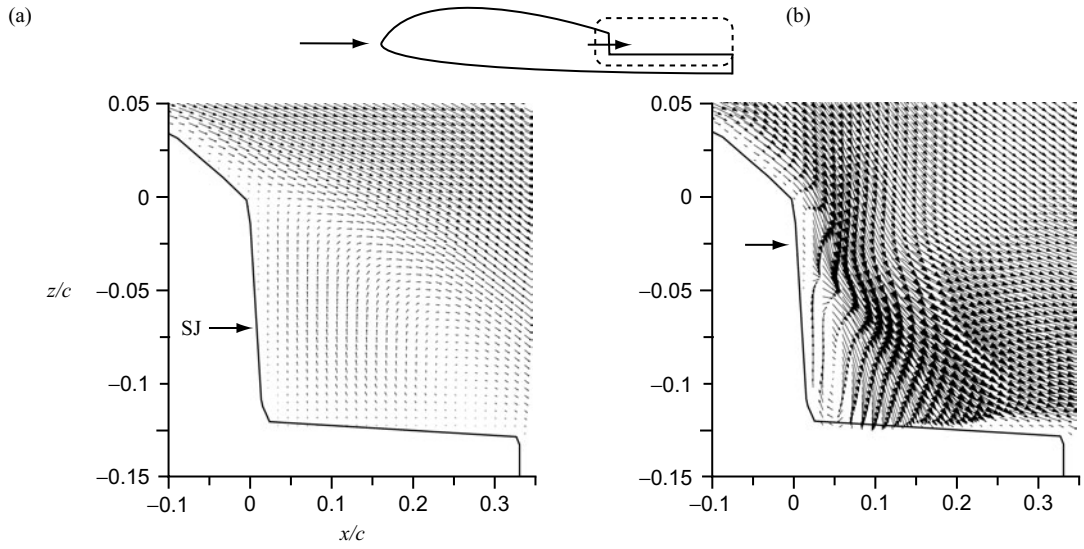

Figure 4. Time-averaged velocity vector fields near the stator's trailing edge. (a) Baseline, and (b) with flow control. $\alpha = 0°$, $\omega = 4{,}200$ RPM.

environment to design and validate the control system. The xPC Target integrates well with Matlab and Simulink, allowing seamless data acquisition and parameter tuning from a host PC running Matlab.

3. RESULTS

The majority of the work presented here focus on the alteration of the flow field around the stators and in their wake due to the activation of the synthetic jet actuators. First, the flow field of the synthetic jet itself is discussed, followed by its effect of the flow field around a stator, and in the wake. As was shown by Fung and Amitay (2002), the flow field downstream of the propeller is radially non-uniform; however, in the present paper only one radial location across the center of the outboard jet ($r/R = 0.43$, marked in a dashed line in Figure 2) is presented as a representative case. Similar effects were obtained at other locations along the stator.

3.1. Synthetic Jet Flow Field

The time- and phase-averaged flow fields of the synthetic jet issued into a quiescence air are presented in Figures 3a and b, respectively (the field of view is marked with a dashed line on the schematics). The time averaged velocity vector field (flow is from top to bottom) exhibits an asymmetric distribution due to the presence of the wall. Fluid is entrained towards the jet orifice and turns into the jet. There is a quasi-steady closed recirculation region near the top left corner and the flow accelerates farther downstream. The phase-averaged flow field is represented by the spanwise vorticity contours (the dashed lines represent negative vorticity, Figure 3b) measured at a phase of 180° (i.e., the beginning of the suction portion of the cycle). Here, the spanwise vorticity is defined as

$$\Omega_z = -\left(\frac{\partial v}{\partial x} - \frac{\partial u}{\partial y}\right) \tag{2}$$

The entrainment towards the jet orifice is clearly visible. Furthermore, the flow field exhibits two (non-symmetric) pairs of counter rotating vortices before they breakdown into a quasi-steady jet.

3.2. Flow Field Over The Stators

The effect of the actuation on the flow field above the surface of the stator vane is investigated using the PIV in the *x*-*y* plane at two angles of attack of 0° and 6° and two propeller rotational speeds of 4,200 and 9,000 RPM. In these experiments, the velocity of the synthetic jet was held constant, resulting in a C_μ of 0.065 and 0.012 for the 4,200 and 9,000 RPM cases, respectively.

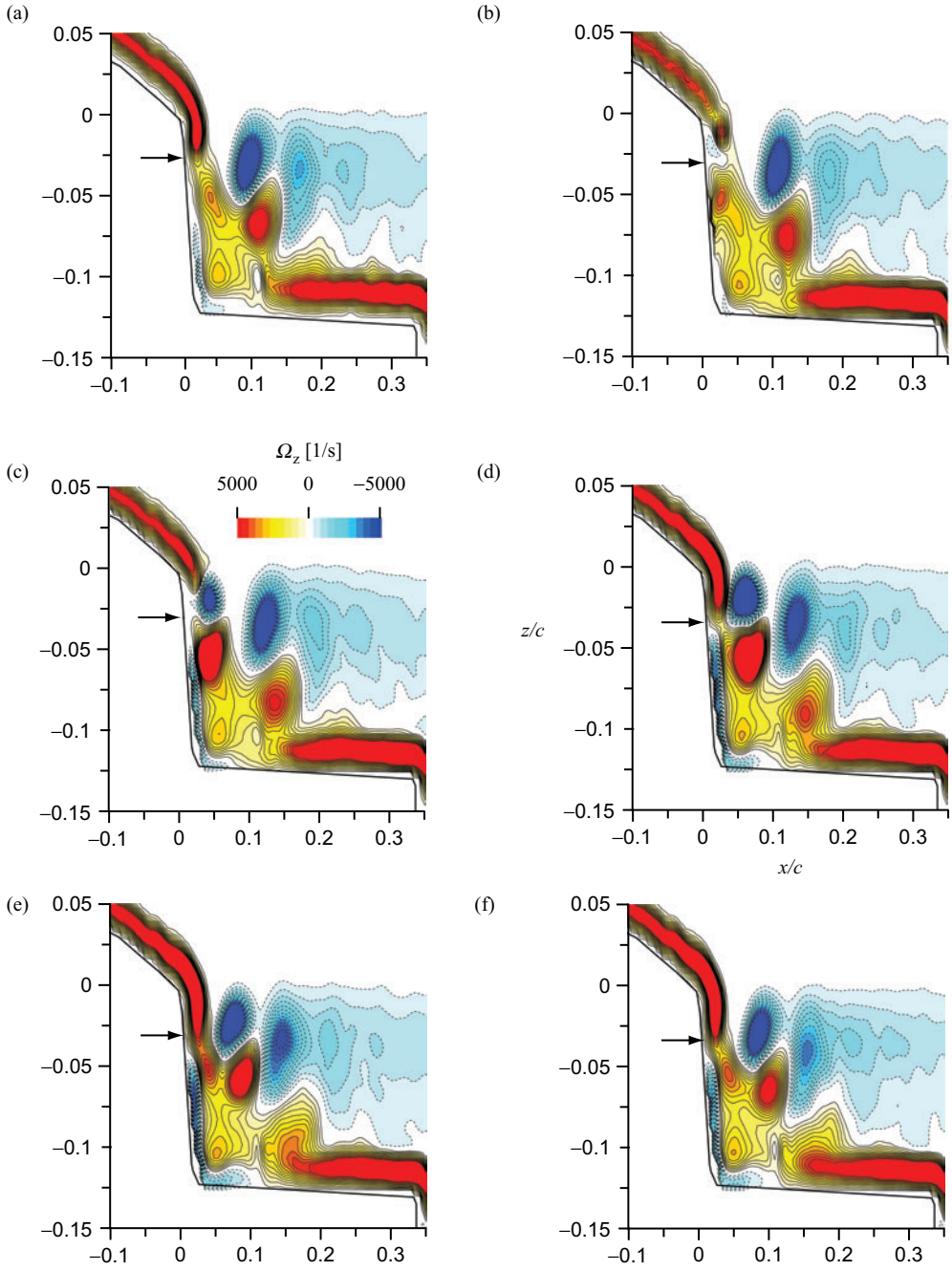

Figure 5. Phase-averaged spanwise vorticity fields for ϕ = a) 0°, b) 60°, c) 120°, d) 180°, e) 240°, f) 300°. α = 0°, ω = 4,200 RPM. Negative vorticity is marked by the dashed lines.

Figure 4 presents the time-averaged velocity vector field of the baseline and actuated cases over the stator (the field of view is marked with a dashed line on the schematics) at an angle of attack of 0°, where the rotational speed is 4,200 RPM. As desired, without flow control (Figure 4a) the flow is fully separated over the ramp. When the synthetic jets are activated, the velocity magnitude is significantly increased throughout the flow field, and separation is almost completely mitigated. This suggests that the activation of the control will result in an increase of lift (and thus, the generation of a yaw moment opposite to the moment generated by the blades' rotation). Furthermore, it is expected that the drag force will be decreased.

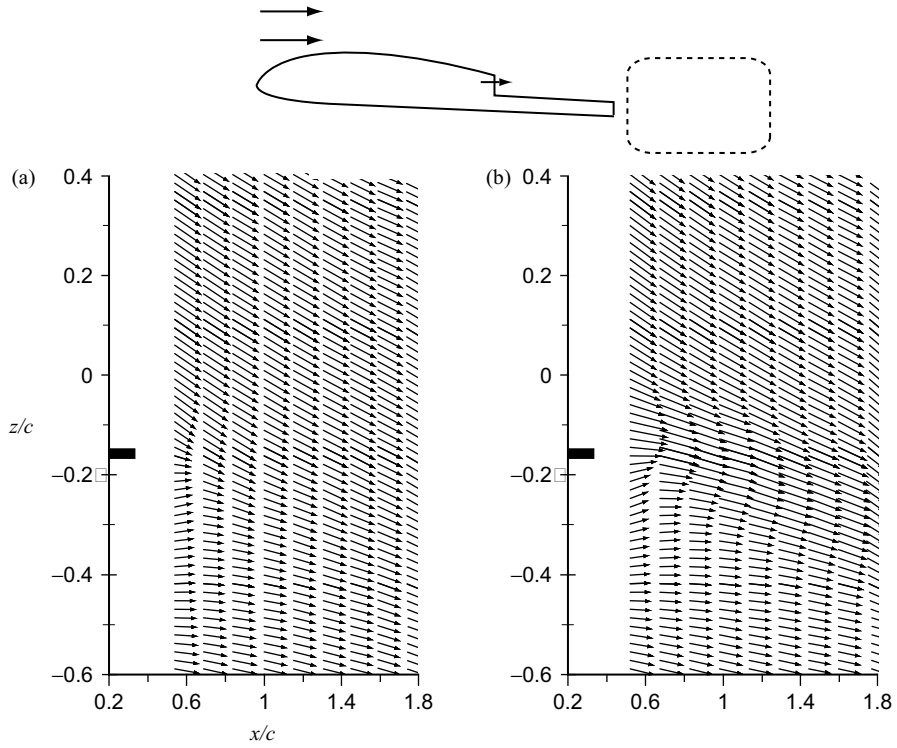

Figure 6. Time-averaged velocity vector fields in the near wake behind the stator. (a) Baseline, and (b) with flow control. $\alpha = 0°$, $\omega = 4{,}200$ RPM.

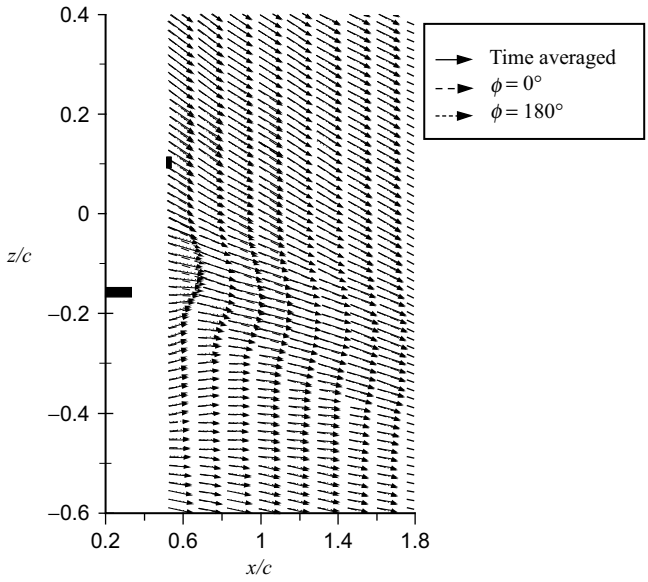

Figure 7. Superimposed time- and phase-averaged velocity vector fields in the near wake behind the stator. (a) Baseline, and (b) with flow control. $\alpha = 0°$, $\omega = 4{,}200$ RPM.

The quasi steady alteration to the flow, observed in the time-averaged data, is formed due to the fact that the actuation frequency is an order of magnitude larger than the characteristic frequency of the flow. In order to understand the formation of the quasi-steady reattachment, data were also acquired phase locked to the actuation cycle of the synthetic jet actuator at six equally-spaced phases, and are presented using the spanwise vorticity in Figures 5a-f (negative, counter clockwise, vorticity is represented by the dashed lines). At $\phi = 0°$ (beginning of blowing portion of the cycle, Figure 5a) the

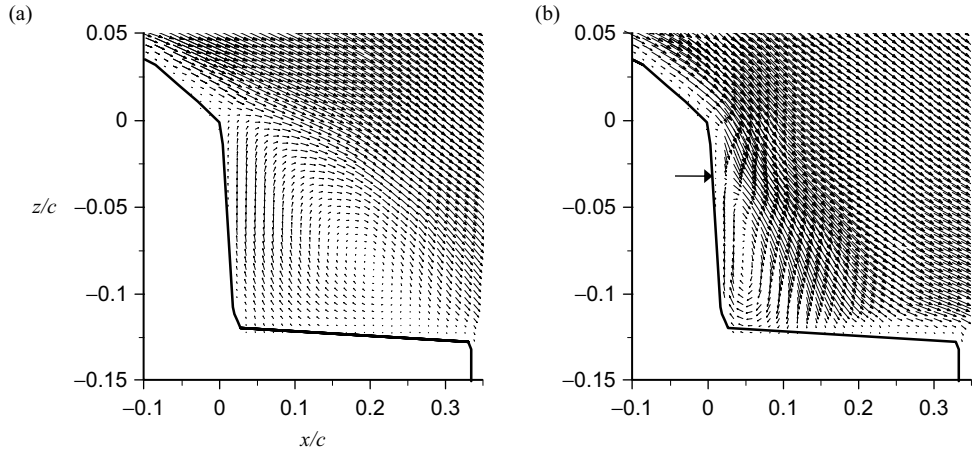

Figure 8. Time-averaged velocity vector fields near the stator's trailing edge. (a) Baseline, and (b) with flow control. $\alpha = 0°$, $\omega = 9{,}000$ RPM.

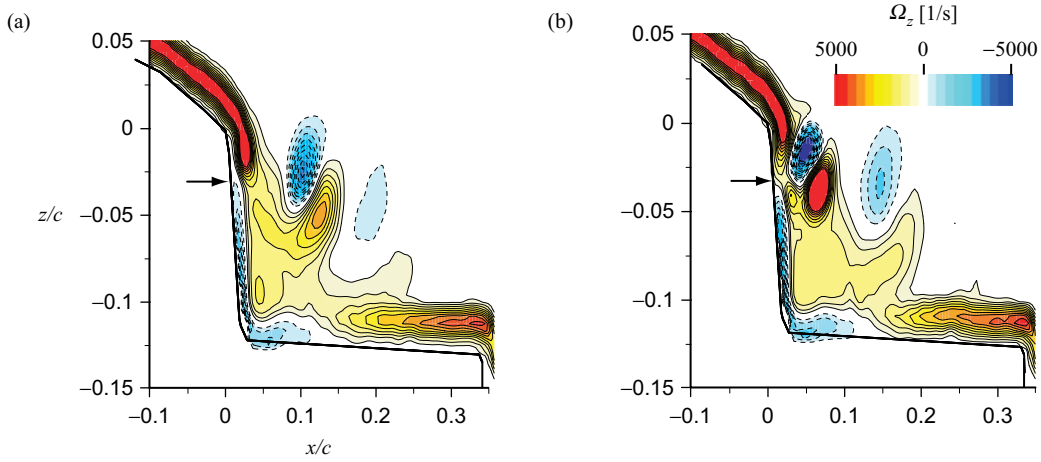

Figure 9. Phase-averaged spanwise vorticity fields for ϕ = a) 0°, b) 180°. $\alpha = 0°$, $\omega = 9{,}000$ RPM. Negative vorticity is marked by the dashed lines.

vorticity field exhibits a pair of counter-rotating vortices at $x/c = 0.1$ that are associated with the previous cycle. Farther downstream the reminiscence of the previous pairs having a much smaller strength can be seen. At $\phi = 60^{o}$ (Figure 5b) a vortex pair is formed near the orifice and is advected downstream as the cycle progresses (Figures 5c-f). Note that the vortex pair are completely diffused at $x/c = 0.3$, suggesting that the reattachment is quasi-steady.

3.3. Near Wake Flow Field

The modification of the flow around the stator vane is accompanied by substantial changes of the stator vane's near wake. Figure 6 presents the time-averaged velocity vector fields for the baseline case (Figure 6a) and the forced case (Figure 6b). As in the previous data set, the angle of attack of the stator vane is fixed at 0°, and $\omega = 4200$ RPM. Without flow control the wake behind the stator is vectored downward due to the generation of lift by the stator. When flow control is applied, the wake distribution exhibits an increase of the velocity behind the stator, suggesting that both lift and thrust have been generated.

As is shown in Figures 5a-f, actuation results in the formation and advection of coherent vortical structures. However, these coherent structures appear to lose their phase coherence (relative to the actuation waveform) before reaching the trailing edge of the stator. This suggests that the controlled wake behind the stator vane is quasi-steady. To validate this assumption the wake in the near field is

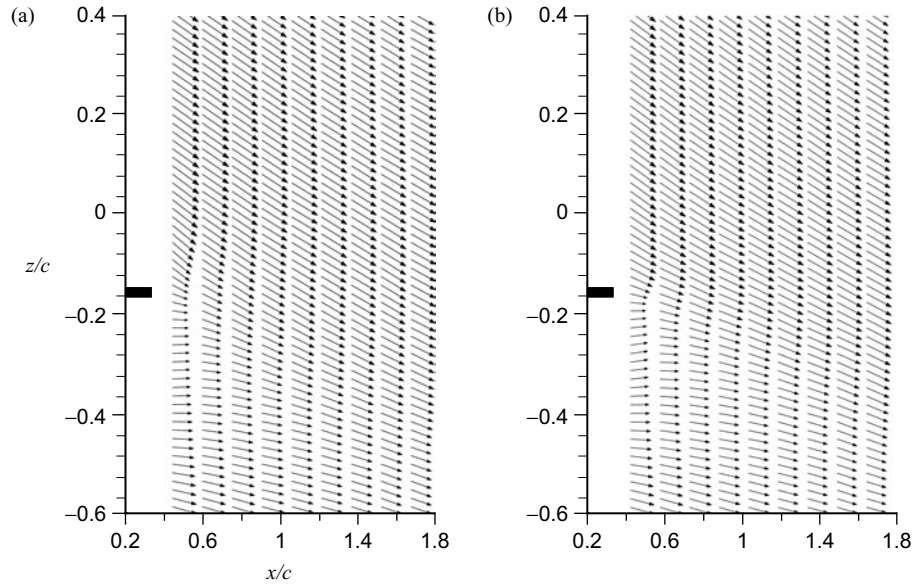

Figure 10. Time-averaged velocity vector fields in the near wake behind the stator. (a) Baseline, and (b) with flow control. $\alpha = 0°$, $\omega = 9{,}000$ RPM.

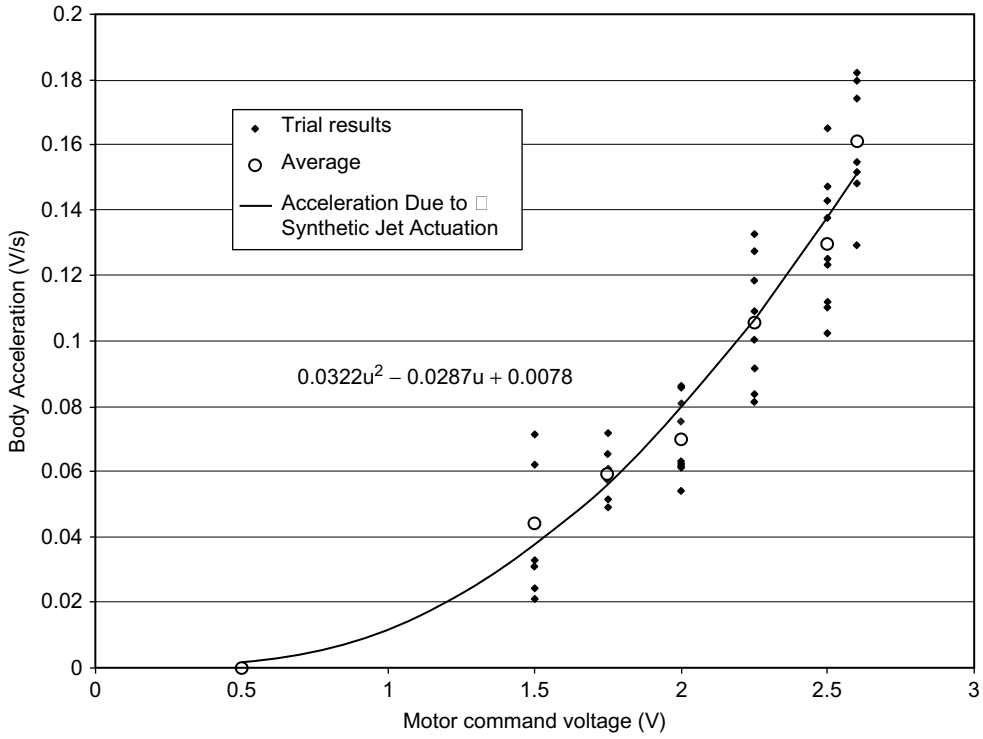

Figure 11. Yaw acceleration resulting from synthetic jet actuation.

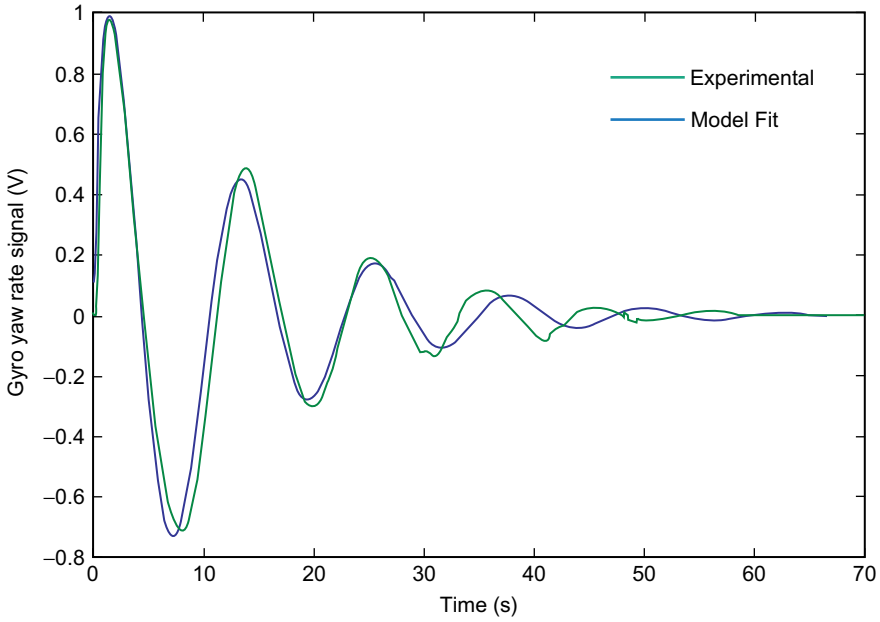

Figure 12. Open-loop system response (green) and model fit (blue) to 0.7 volt step input in motor command

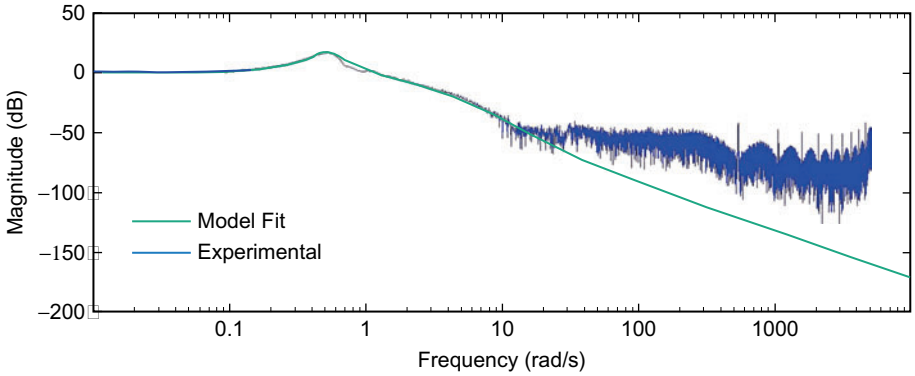

Figure 13. Frequency response of experimental (blue) and identified (green) systems.

measured phase-locked to the actuation signal and compared to the time-averaged flow field. Figure 7 presents the superimposed time-averaged and phase-averaged velocity vector fields at two phases ($\phi = 0^o$ and 180^o) in the near wake of the stator vane. Clearly, the time-averaged and phase-averaged vector fields are almost indistinguishable suggesting that the wake behind the stator vane (and the aerodynamics forces) is indeed quasi-steady.

As mentioned above, the effectiveness of the flow control was also examined at a higher rotational speed of 9,000 RPM and the results are presented in Figures 8-10. Figure 8 presents the time-averaged velocity vector field of the baseline and actuated cases over the stator at an angle of attack of 0^o. The baseline case (Figure 8a) exhibits a fully separated flow over the ramp. When flow control is activated, the extent of the separated region is significantly reduced (although it is not as pronounced at the former case where $\omega = 4{,}200$ RPM). Note that the velocity of the synthetic jet was held fixed and thus the momentum coefficient of the synthetic jet for the $\omega = 9{,}000$ RPM case is smaller than the lower rotational speed case.

Figure 9 presents the phase averaged vorticity field at $\phi = 0^o$ (beginning of blowing portion of the cycle, Figure 9a) and at $\phi = 180^o$ (beginning of the suction portion of the cycle, Figure 9b). The vorticity field exhibits similar vortical structures as for the lower rotational speed case. However, the vortices loose their coherence close to the ramp (after ~2 cycles) and the flow seems to be time-invariant for $x/c > 0.25$.

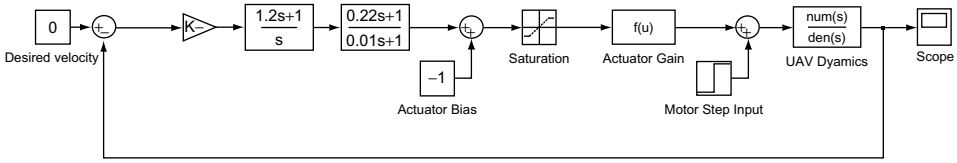

Figure 14. Block diagram of controller simulation.

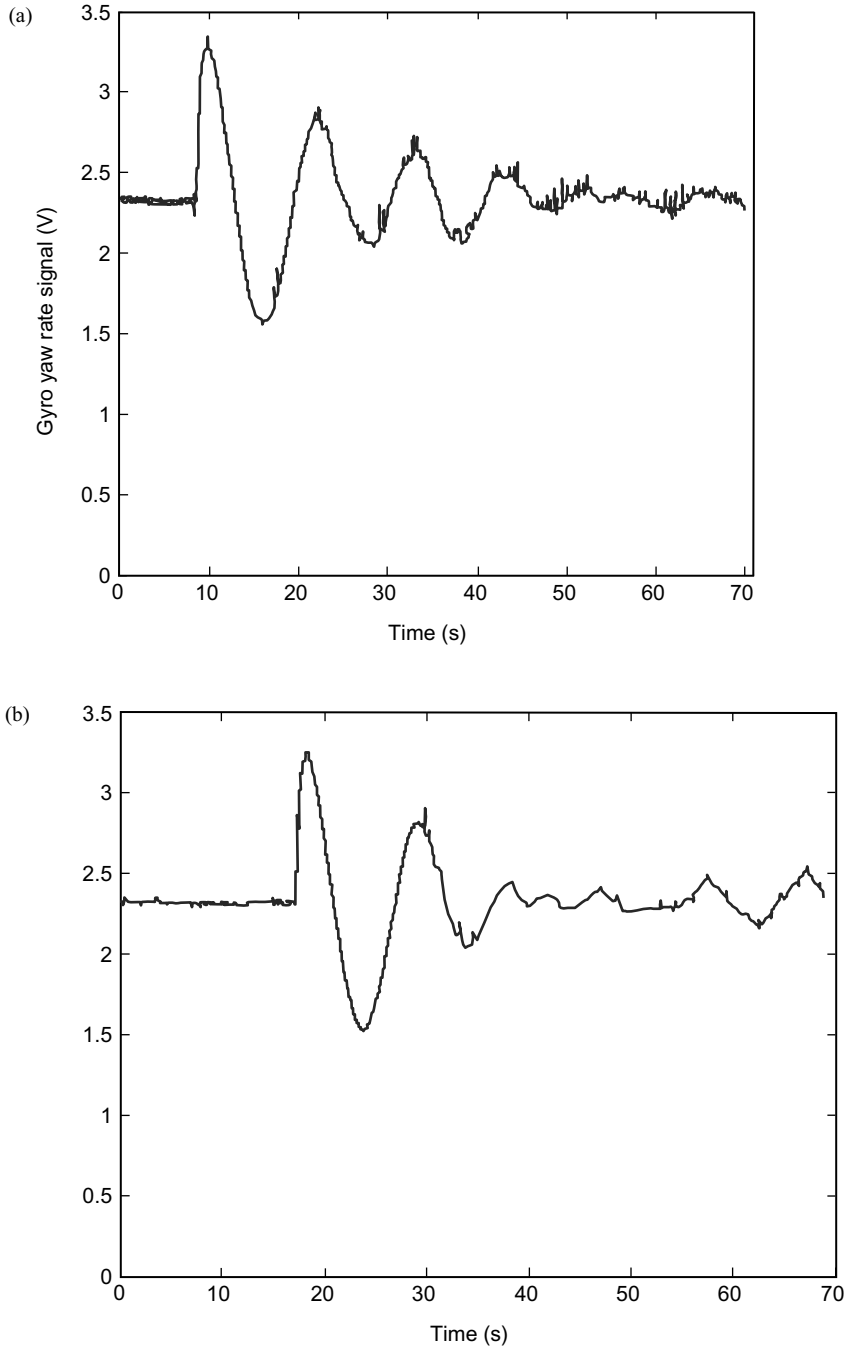

Figure 15. Experimental response – 0.7 volt step input: (a) without flow control, and (b) with closed-loop flow control.

Finally, Figure 10 presents the near wake with and without flow control. As can be seen, the effect of flow control on the wake is smaller than for the lower rotational speed case. Still, the wake deficit is reduced and the velocity magnitude at the upper portion of the wake is increased compared to the baseline case. It is noteworthy that similar results were obtained when the stators were oriented at 6° with respect to the flow and are not shown here for brevity.

It is noteworthy that the velocity and vorticity data presented in this paper is to prove that the synthetic jets can alter the flow field over the stators. In the future we plan to use these data to obtain a low order model of the flow, which can then be used for closed-loop control.

3.4 Closed-Loop Control

The objective defined for the closed-loop control system is to regulate the yaw rate to zero in the presence of disturbances. In this paper, disturbances are introduced to the system by applying a rapid change to the rotor speed, which produces an undesirable yaw moment. It is desirable to reduce both the peak amplitude of the oscillation induced by this moment, as well as the settling time of the oscillation. The procedure of identifying the dynamic model of the vehicle and designing the controller will be described, and results are presented in this section.

Before designing a closed-loop controller, a model describing the dynamics of the vehicle must be obtained. This model can be obtained from first principles or from data-driven system identification techniques; often an initial model is obtained from first principles and then calibrated to the experiment using system identification techniques. This procedure was used in the current design.

A second-order dynamic model of a rotational system was assumed, with initial values selected for the mass moment of inertia, J, and damping constant, B. This model is shown in VanOverschee & DeMoor (1996) in transfer function form. Note that a small stiffness term, K, was also included to account for the elasticity of the test fixture. The model states are position and rotation about the vertical axis. The input to the model is yaw torque, $T(s)$ and the output is the yaw angular position, $\theta(s)$.

$$\frac{\theta(s)}{T(s)} = \frac{\frac{1}{J}}{s^2 + \frac{B}{J}s + \frac{K}{J}} \tag{3}$$

From our previous work, the yaw torque supplied by the synthetic jet actuators is a nonlinear function of applied voltage. To successfully apply linear control design techniques to the vehicle, this nonlinear relationship can be identified and inverted to linearize the voltage-to-torque characteristic. The relationship was found by applying several input voltage values to the motor and observing the vehicle acceleration that results. The yaw acceleration will reach a constant value and then begin to decay as an opposing moment is applied due to the damping and spring deflection. The acceleration measured during the initial rotation (when spring deflection and dissipative damping are small) was used to compute the jet relationship. The result is a quadratic function as shown in Figure 11.

With initial values derived from first principals, system identification techniques were then used to determine the model constants that best describe the experimental system. A subspace identifcation algorithm (VanOverschee & DeMoor, 1996) was used to determine these parameters in Matlab. The step response of the resulting system and the corresponding experimental result are shown in Figure 12. The frequency response plots of the identified and experimental systems are shown in Figure 13. It can be seen that the responses match well in the time domain and also in the frequency domain of interest; therefore a second-order system is sufficient to describe the system dynamics.

With a dynamic model identified, control design can proceed. Initially, a classic Proportional-Integral-Derivative controller was used. Using Matlab's linear control design tools, a root locus technique was applied to place the closed-loop poles for faster settling time and reduced overshoot

$$\text{Final PID Controller}: \frac{1.7547(1.2s+1)(0.22s+1)}{s(0.01s+1)} \tag{4}$$

This controller was implemented in Simulink and simulated with a step disturbance as shown in Figure 14. After the controller was successfully validated for acceptable performance, Real-Time Workshop was used to convert it to an executable application to run on the xPC target platform. The output of the

linear controller was routed through an algebraic function that inverts the quadratic voltage-to-acceleration relationship shown in Figure 11, so that the dynamics of the controlled system are more linear. A bias was also applied for the electronics, as shown in Figure 14.

The results of the closed-loop control implementation appear in Figures 15a and b, which show the unactuated and actuated cases, respectively. The results show a clear reduction in settling time as anticipated. The main limitation in performance in this system is the low control authority of the jet actuators. Even when maximum voltage is applied to the actuators, the resulting yaw moment was relatively small, resulting in low effectiveness until the oscillation amplitude decays. Saturation of the control signal was also an issue, since the controller gain was relatively high to achieve the desired performance.

4. CONCLUSIONS

The present paper presents an active flow control-base technique to stabilize a micro ducted fan unmanned aerial vehicle in a yaw motion. Synthetic jet actuators, placed in the stators, were used to control the flow over the stators. As a result, this mechanically simplified control approach can be used to generate a yaw moment (and in the future, pitch and roll moments) on the vehicle instead of moving control surfaces and articulated rotor blades.

At the present work, four stators were placed downstream of the propeller. Adding more stators will probably increase the control authority; however it may also increase the drag on the stators and thus reduce the effective thrust. This will be examined in a future work.

The flow field around the stators and in the near wake was studied using particle image velocimetry at two angles of attacks and two rotor rotational speeds. Without flow control, the flow over the stators was deliberately separated near the trailing edge. When the synthetic jets were activated, the velocity magnitude was significantly increased throughout the flow field, and separation was almost completely mitigated. This suggests that the activation of the control will result in an increase of lift (and thus, the generation of a yaw moment opposite to the moment generated by the blades' rotation). Furthermore, it is expected that the drag force will be decreased.

The quasi steady alteration to the flow is formed due to the high actuation frequency, which is an order of magnitude larger than the characteristic frequency of the flow. This was examined by measuring the phase-locked vorticity field at different phases. It was found that the vortical structures (associated with the synthetic jet) defuse before reaching the stator's trailing edge. Furthermore, the near wake is quasi-steady.

A closed-loop controller with a gyroscopic feedback was implemented to regulate the yaw rate to zero and reject disturbances caused by changes in propeller speed. The benefits of closed-loop control design for yaw control of a micro unmanned air vehicle were presented. Even with the limitations of control authority presented by these actuators, a significant effect is seen when considering the settling time of the yaw rate in response to a step moment disturbance input. It is therefore anticipated that with appropriate changes to the actuators the performance will be substantially increased.

REFERENCES

1. Adams, N., Biagioni, M. and Lipera, L., "A VTOL Micro Air Vehicle Design Concept and Projected Mission Utility", Micro Craft Inc., San Diego, CA, 2001.
2. Amitay, M. and Cannelle, F., "Evolution of Finite Span Synthetic Jets", *Physics of Fluids*, Volume 18, Issue 5, 2006.
3. Amitay, M., Horvath, M., Michaux, M., and Glezer, A. "Virtual Aerodynamic Shape Modification at Low Angles of Attack using Synthetic Jet Actuators", AIAA Paper 2001-2975, 2001.
4. Amitay, M., Smith, D.R., Kibens, V., Parekh, D.E. and Glezer, A., "Modification of the Aerodynamics Characteristics of an Unconventional Airfoil Using Synthetic Jet Actuators", *AIAA Journal*, Vol. 39, No. 3, pp. 361-370, March 2001.
5. Chatlynne, E., Rumigny, N., Amitay, M. and Glezer, A., "Virtual Aero-Shaping of a Clark-Y Airfoil Using Synthetic Jet Actuators", AIAA Paper 2001-0732, 2001.
6. Cycon, J.P., "Sikorsky Aircraft UAV Program", *Vertiflite*, **38**(3), pp. 26 – 30, 1992.
7. Fung, P., and Amitay, M., "Active Flow Control Application on a Mini Ducted Fan UAV", *Journal of Aircraft*, Vol. 39, No. 4, pp. 561-571, 2002.
8. Glezer, A. and Amitay, M., "Synthetic Jets", *Annual Review of Fluid Mechanics*, **34**, 2002.
9. Kondor, S. and Heiges, M., "Active Flow Control For Control of Ducted Rotor System", AIAA

Paper 2001-0117, 2001.

10. Smith, B.L., Glezer, A., "The formation and evolution of synthetic jets", Physics of Fluids. 31:2281-97, 1998.
11. VanOverschee, P., and B. DeMoor, "Subspace Identification of Linear Systems: Theory, Implementation, Applications", Kluwer Academic Publishers, 1996.
12. Walsh, D. and Cycon, J.P., "The Sikorsky Cypher® UAV: A Multi-Purpose Platform with Demonstrated Mission Flexibility", American Helicopter Society 54th Annual Forum, Washington, D.C., 1998.